

Tumor viability evaluation by positron emission tomography with [^{18}F]FDG in the liver metastasis rat model

Kiichi ISHIWATA,* Han-yu LIU,** Kenichi TERAMOTO,** Kazunori KAWAMURA,*
Keiichi ODA* and Shigeki ARII**

*Positron Medical Center, Tokyo Metropolitan Institute of Gerontology

**Department of Hepato-Biliary-Pancreatic Surgery, Tokyo Medical and Dental University

We prepared a liver metastatic tumor model by injection of rat colon adenocarcinoma cells to Fischer F344 rats through portal vein, and applied positron emission tomography (PET) using 2-deoxy-2-[^{18}F]fluoro-D-glucose ([^{18}F]FDG) ([^{18}F]FDG-PET) to this model. At an early stage of the model, multiple small tumor nodules appeared in the inferior lobes of the livers, and extended later into the superior lobes. To evaluate the tumor growth and tumor viability at the early stage, we proposed a new concept, tumor viability index (TVI), instead of the standardized uptake value (SUV) of the [^{18}F]FDG uptake. The TVI was defined by subtracting the signal based on the normal liver from the total signal in the whole liver including tumor nodules: (whole liver SUV – normal liver SUV) \times ml of whole liver region of interest (ROI). For the signal of the whole liver, ROIs were placed on six slices covering the whole liver, and the ROI of normal liver region was located in the superior lobe of the liver. The average TVI values increased with tumor growth and significantly correlated with the numbers of tumor nodules. The new concept may be useful for evaluating the tumor viability non-invasively and quantitatively by [^{18}F]FDG-PET.

Key words: Tumor viability index, liver metastasis, PET, [^{18}F]FDG

INTRODUCTION

POSITRON EMISSION TOMOGRAPHY (PET) with 2-deoxy-2-[^{18}F]fluoro-D-glucose ([^{18}F]FDG) ([^{18}F]FDG-PET) is widely used for tumor diagnosis by focusing on early detection of malignant tumors and on measurement of tumor viability to evaluate the therapeutic effects.¹ The liver is the most common site of metastasis of gastrointestinal cancer and nearly half of all patients with primary colorectal cancer ultimately develop liver metastases during the course of their disease.^{2,3} Patients with liver metastasis require chemotherapy in inoperable cases, and it is of great importance to evaluate properly whether the treatment of such patients has been done.^{4,5} Therapeutic efficacy in such patients is usually judged by a reduction

in tumor size; however, [^{18}F]FDG-PET is probably more suitable for evaluating the tumor viability, because [^{18}F]FDG uptake by tumor tissues was correlated well with the viable tumor cells¹ and because the reduction in [^{18}F]FDG uptake proceeded much faster than the morphological change following radiotherapy of experimental tumors.^{1,6} In experimental studies, [^{18}F]FDG-PET using the liver metastatic tumor model could be also of use for the development of the new therapeutic protocols. Recent advanced high-resolution PET scanners enable visualization of small tumors in animal models.^{7–11} However, it may be still difficult to visualize multiple small tumor nodules in animal models. [^{18}F]FDG-PET had the ability to detect only 35% of small nodules less than 2 mm in diameter.¹²

We are interested in the development of new therapeutic protocols for liver metastasis by application of [^{18}F]FDG-PET to experimental animal models. In this study, we developed a liver metastatic tumor model, in which numerous small nodules appeared in the inferior lobes of the livers. The animal PET scanner used in our

Received February 15, 2006, revision accepted May 8, 2006.

For reprint contact: Kiichi Ishiwata, Ph.D., Positron Medical Center, Tokyo Metropolitan Institute of Gerontology, 1–1 Nakacho, Itabashi-ku, Tokyo 173–0022, JAPAN.

E-mail: ishiwata@pet.tmig.or.jp

Table 1 Rat groups used and experimental protocols

Experimental group	Examination Day*	PET Scan mode	Other examination
1. Primary tumor-bearing rats (8 wo, 1×10^7)**	35		Tissue dissection (16)***
2. Metastatic tumor-bearing group 1 (8 wo, $0.1-1 \times 10^7$)**	27-42		Nodule number (22)***
3. Metastatic tumor-bearing group 2 (8 wo, 1×10^7)**	27		<i>Ex vivo</i> autoradiography (2)*** Anatomical slice (1)
4. Metastatic tumor-bearing group 3 (8 wo, 1×10^7)**	35	Dynamic scan (2)*** Static scan (3)***	Tissue dissection (5)***
5. Metastatic tumor-bearing group 4 (8 wo, 1×10^7)**	18	Static scan (6)***	Nodule number (6)***
6. Metastatic tumor-bearing group 5 (6 wo, 0.5×10^7)**	27	Static scan (8)***	Nodule number (8)***
7. Control rats (8 wo, none)**	16	Static scan (4)***	Anatomical slice (1)

*Day after tumor inoculation. **Age (weeks old) at the injection of tumor cells and number of tumor cells injected in the parentheses.

***Number of rats in the parentheses.

Table 2 Number of tumor nodules after injection of RCN-9 cells into a portal vein in male Fisher 344 rats

Tumor inoculation		Tumor nodule number	
Cell number	Week (n)*	≤ 3 mm	> 3 mm
0.1×10^7	4 (3)	None	None
0.5×10^7	4 (4)	1.8 ± 2.9	1.5 ± 1.7
1.0×10^7	4 (3)	16.3 ± 20.6	3.7 ± 3.2
1.0×10^7	5 (6)	31.7 ± 42.7	6.8 ± 2.9
1.0×10^7	6 (6)	77.0 ± 88.9	16.5 ± 14.4

*Number of rats.

laboratory,^{13,14} however, has relatively low spatial resolution (3.5 mm full width at half maximum)¹⁴ compared with the recent advanced PET scanners. To measure quantitatively [¹⁸F]FDG uptake by tumor tissues, the standardized uptake value (SUV) has often been used. By applying [¹⁸F]FDG-PET to the metastasis model, however, we intend to evaluate the tumor viability during treatments to confirm the therapeutic effects, but not to simply detect localization of tumors or to compare their [¹⁸F]FDG uptake. Therefore, we propose the tumor viability index (TVI) as a new concept which reflects whole signals from [¹⁸F]FDG taken up by all tumor tissues including multiple and small tumor nodules. Here we validated the TVI in the liver metastatic tumor model.

MATERIALS AND METHODS

All animal studies were approved by the Animal Care and Use Committee of the Tokyo Metropolitan Institute of Gerontology, and by the Tokyo Medical and Dental University Care and Use Committee. Male Fisher F344/DuCrj rats were purchased from SLC Inc. (Shizuoka, Japan). The rat model with liver metastasis was prepared at the animal experiment center of Tokyo Medical and Dental University, and housed in an air-conditioned, light-controlled environment (22°C, 12-hour light and 12-hour dark conditions) with free access to food and

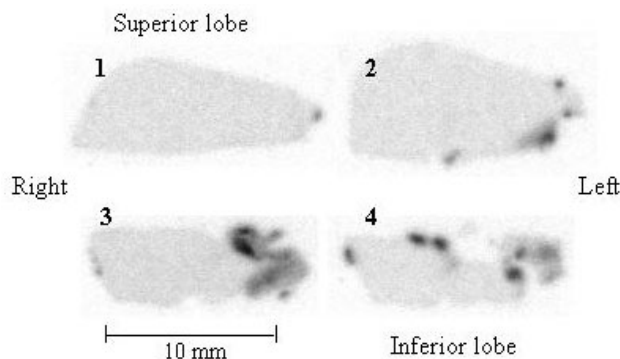


Fig. 1 *Ex vivo* autoradiograms of the liver sections 120 min after intravenous injection of [¹⁸F]FDG into the rat in the metastatic tumor-bearing group 2. Four slices from superior lobe to inferior lobe are demonstrated.

water. The rat colon adenocarcinoma cell line (RCN-9) was provided by Kyoto University. The cells were cultured as previously described.¹⁶ PET studies were performed at the Positron Medical Center of the Tokyo Metropolitan Institute of Gerontology. [¹⁸F]FDG was prepared by using FDG MicroLab (GE Medical Systems, Uppsala, Sweden).

Preparation of the rat tumor model

Two tumor models were prepared. One is a primary tumor model, in which the suspension of RCN-9 cells in 0.2 ml phosphate-buffered saline (PBS) containing 1×10^7 cells was subcutaneously injected in the thigh of 8-week-old rats and inoculated for 35 days ($n = 16$). The other is a metastasis model. Rats (6-8 weeks old, $n = 47$) were treated with a midline subxyphoid incision under ether anaesthesia. The suspension of RCN-9 cells in PBS ($0.1-1 \times 10^7$ cells/1 ml) was injected into rats via portal vein ($n = 44$) and as the control group ($n = 4$) 1 ml PBS was given into the other group of rats via portal vein. Rat groups used and experimental protocols are summarized in Table 1.

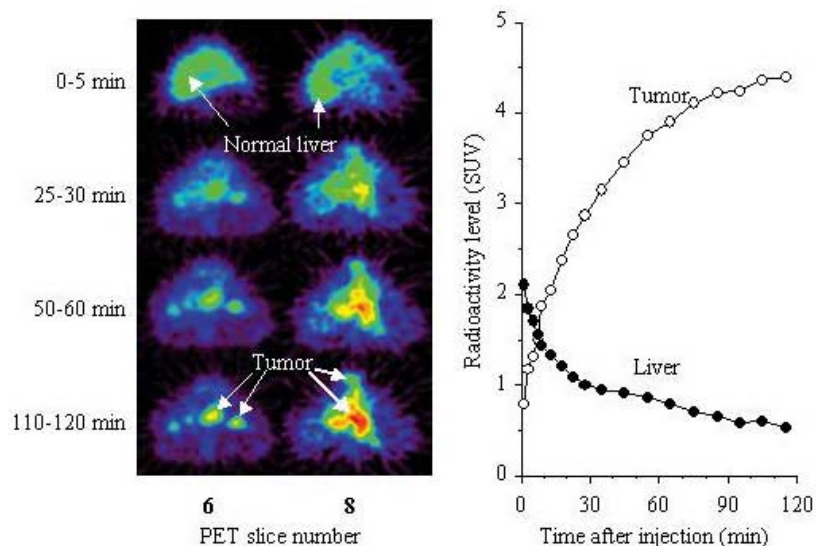


Fig. 2 Sequential PET images and the time-activity curves of tumor and normal liver regions after intravenous injection of [¹⁸F]FDG into the rat in the metastatic tumor-bearing group 3. The circular ROIs of the tumor (*open circle*) and normal liver (*solid circle*) were placed on the hot area in the 8th slice and the cold area in the 5th slice (not shown), respectively. The uptake level of [¹⁸F]FDG was expressed as the standardized uptake value (SUV).

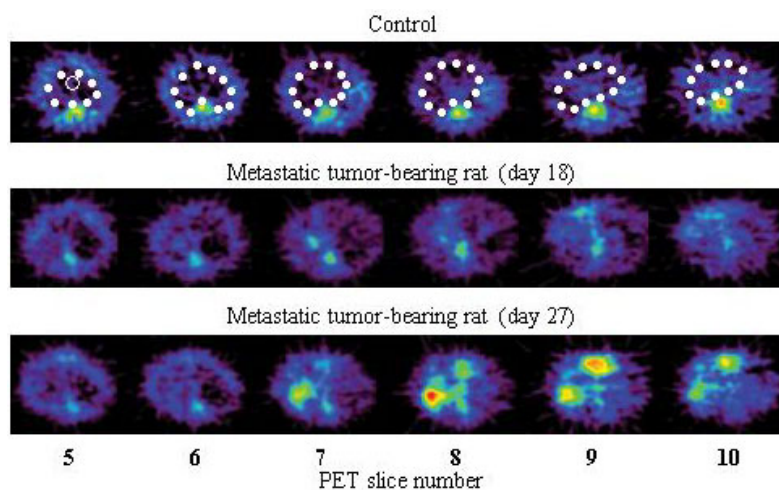


Fig. 3 PET images of the control and metastatic tumor-bearing rats. The ROIs on the whole liver are shown in dotted lines, and an open circle in the 5th slice represents the ROI of normal liver region.

Tumor growth in the metastatic tumor model

Rats in the metastatic tumor-bearing group 1 were divided into five subgroups ($n = 3-6$) and were killed by cervical dislocation 4, 5 or 6 weeks after injection of RCN-9 cells ($0.1, 0.5$ or 1×10^7 cells) via portal vein. The whole liver was dissected and the number of tumor nodules on the surface of the liver was counted.

Tissue dissection study

The time-courses of [¹⁸F]FDG in the liver and surrounding organs in the thoracic and abdominal regions were determined by tissue dissection methods using the pri-

mary tumor model 5 weeks after subcutaneous injection of tumor cells. [¹⁸F]FDG (5 MBq) was intravenously injected into rats without fasting via tail vein and they were killed by cervical dislocation 30, 60, 120 and 240 min postinjection ($n = 4$). The blood was collected by heart puncture, and tumor, lung, liver, pancreas, spleen, small intestine and kidney were dissected. In the metastatic tumor-bearing group 3, immediately after the PET scan (120 min postinjection), the rats were killed by cervical dislocation, and tumor nodules and normal liver region were dissected. The samples were measured for radioactivity with an auto-gamma counter and then

Table 3 Comparison of [^{18}F]FDG uptake in tumor and normal liver evaluated by PET and tissue dissection in the rats of the metastatic tumor-bearing group 3

	PET (n = 5)		Tissue dissection (n = 5)	
	Uptake (SUV)	Tumor/liver ratio	Uptake (SUV)	Tumor/liver ratio
Tumor	2.11 \pm 0.81*		3.87 \pm 0.76	
Liver	0.26 \pm 0.08	8.1 \pm 1.5	0.24 \pm 0.07	16.8 \pm 3.6

* [^{18}F]FDG uptake was not determined by static PET scan alone at 110–120 min after the tracer injection. Immediately after the PET scan, tissue dissection was carried out.

Table 4 Tumor viability index (TVI) measured by [^{18}F]FDG-PET and the numbers of tumor nodules in the rats of the metastatic tumor-bearing groups 4 and 5

Group	PET measurement		Nodule number
	Day*	TVI SUV \times ml	
Metastasis tumor-bearing group 4	18 (6)	0.69 \pm 0.37	13.5 \pm 10.6
Metastasis tumor-bearing group 5	27 (8)	1.86 \pm 1.09	23.8 \pm 16.7
Control rats	14 (4)	0.24 \pm 0.03	none

*Day after inoculation of tumor cells and the numbers of rat used in the parentheses.

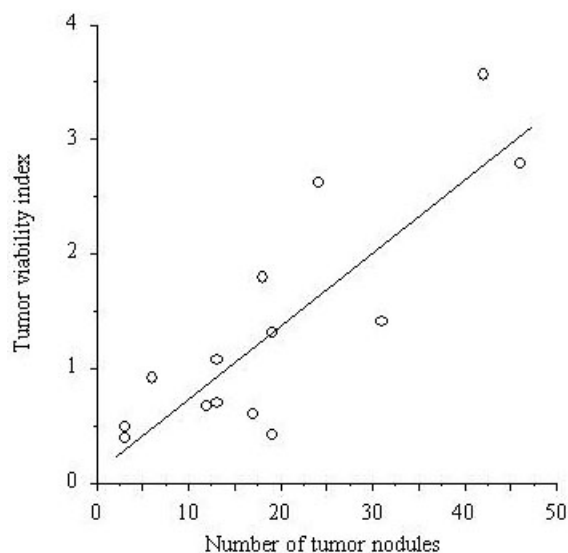


Fig. 4 Relationship between tumor viability index values and numbers of tumor nodules of 14 rats in the metastatic tumor-bearing groups 4 (day 18) and 5 (day 27). The Statistical Package for the Social Sciences (SPSS) v10.1 (Chicago, IL, USA) was used to analyze the data. Significant relationship was observed between the two indices ($r = 0.763$; $p = 0.002$).

weighed. The uptake of [^{18}F]FDG was expressed as the standardized uptake value [SUV, (activity of sample/g of sample)/(total injected activity/g body weight)].

Ex vivo autoradiography of the liver with tumor nodules [^{18}F]FDG (18 MBq) was intravenously injected into two rats in the metastatic tumor-bearing group 2 at 27 days after tumor inoculation (Table 1). The rats were killed by

cervical dislocation 120 min later and *ex vivo* autoradiography of the liver was performed as described previously.¹⁷ The left lobe of the liver was dissected, frozen and cut into 30 μm -thickness using a cryotome (Bright Instrument Co. Ltd., Huntingdon, UK). The liver sections were dried on a hot plate at 60°C and apposed to a storage phosphor screen (Phosphor Imager SI system, Molecular Dynamics, Sunnyvale, CA, USA), and the distribution of [^{18}F]FDG was visualized.

PET study

The animal PET scanner used was SHR-2000 model (Hamamatsu Photonics K.K., Hamamatsu, Japan). The camera provides a set of 14-slice images at center-to-center intervals of 3.25 mm in Z-2 motion with image-spatial resolution of 3.5 mm full width at half maximum.¹⁵ An axial resolution was 5.0 mm full width at half maximum. The administered dose of [^{18}F]FDG was 10–20 MBq.

Positioning of rats in the PET scanner: The rat, which was fasted overnight before the PET study, was anesthetized with isoflurane (2.0%) and was fixed supine on the bed of the PET scanner. The place at 20-mm distance apart from xiphoid angle to the abdomen was positioned at the seventh slice from the rostral side. The seventh slice approximately corresponded to the center of the liver, and the 14-slice interval (42.25 mm) covered from the bottom of the heart to the kidney at a rough estimate.

Dynamic PET scan: To measure the time-courses of [^{18}F]FDG in tumor and liver and to locate the region of liver, dynamic PET scan was performed in two metastatic tumor-bearing rats of group 3 (Table 1). After transmission scanning with a rotating [^{68}Ge]/[^{68}Ga] line source for

10 min to correct for attenuation, [^{18}F]FDG was intravenously injected into rats through tail vein, and a time sequential tomographic scan was carried out for 120 min (90 frames by 1 min and 6 frames by 5 min).

Static PET scan: To investigate tumor uptake of [^{18}F]FDG in several rats on the same day, static PET scan was performed (groups 3–5 in Table 1). All rats in each group successively underwent 10-min transmission scanning under isoflurane-anaesthesia to correct for attenuation as described above. Then, they were recovered in a conscious state. [^{18}F]FDG was intravenously injected into each of the conscious rats at approximately 25-min intervals, and 100 min later the rat was again fixed on the same position of the PET scanner under isoflurane-anaesthesia. Then, 10-min PET scan was started 110 min after the tracer injection. After the PET scan, the rats of groups 4 and 5 were killed and the numbers of tumor nodules on the surface of the livers were counted.

Evaluation of PET data

To locate the regions of interest (ROIs) on tumor and liver tissues, a rat with liver metastasis in group 2 and a control rat after the static PET scan were frozen and cut horizontally at the corresponding slice positions of PET imaging to make the anatomical slices for setting ROIs on the liver.

Tumor uptake of [^{18}F]FDG determined by SUV: The uptake of radioactivity in the normal liver and tumor regions was determined. The ROI on the normal liver region was placed on the fifth slice by dissection after the PET scan and by referring the photographs of anatomical slices of the rat body, because most of the tumor nodules appeared in the inferior lobe of liver and hardly extended into the superior lobe during the five-week period investigated. The ROI on the tumor was located on the hot spot in the later images. The decay-corrected radioactivity in these ROIs was expressed as the SUV, (activity in ROI/ml of ROI)/(total injected activity/g body weight).

Tumor viability index (TVI): Because of the spatial resolution of the PET scanner used, it is very difficult to detect small and multiple tumor nodules and to discriminate tumor nodules from the normal liver region and surrounding tissues. Therefore, [^{18}F]FDG uptake by all tumor nodules in the liver was evaluated by subtracting the signal based on the normal liver from the total signal in the whole liver including tumor nodules and defined as the TVI.

In the set of 14 slices images, the fifth to tenth slices from the rostral side covered most of the liver. For the total signal in the whole liver including tumor tissues, large ROIs were placed on the regions covering the whole liver in the fifth to tenth slices in comparison with the anatomical slices of the rats (photographs, not shown). The uptake values of radioactivity (SUV_{wl}) and volume (ml) of each ROI in the six slices were determined. Therefore, SUV_{wl} contained the radioactivity of mainly normal liver and tumor tissues and the surrounding tissues in part. For the

signal in normal liver, the ROI was placed on the superior lobe of the liver in the fifth slice as described above and the uptake value of radioactivity (SUV_{nl}) was determined. Then, the signal based on all tumor nodules in each slice was calculated as the $(\text{SUV}_{\text{wl}} - \text{SUV}_{\text{nl}}) \times (\text{ml of liver ROI})$, and the summed signal in the six slices (from fifth to tenth slices) was defined as the TVI.

RESULTS AND DISCUSSION

In the liver metastasis model, the numbers of tumor nodules increased with the numbers of tumor cells injected and with the period inoculated; however, it was noticed that this model had a large variation (Table 2). In the early stage, the tumor nodules were mainly observed in the inferior lobes of the livers and expanded later into the superior lobes. This characteristic of distribution and extension of tumor nodules is due to the preparation method that the tumor cells were injected into portal vein. Therefore, when this metastasis model will be applied to investigation of the therapeutic effects of the treatments of tumors, the preferable period would be 4 to 6 weeks after the injection of 1×10^7 tumor cells. Several large nodules at the later stage had necrotic regions. Thus, we investigated whether the [^{18}F]FDG-PET using an animal PET scanner can evaluate the tumor growth or tumor viability during 5 weeks after inoculation of tumor cells.

First, time-courses of the radioactivity levels in the liver, surrounding normal tissues and tumor for 240 min after injection of [^{18}F]FDG were investigated in the primary tumor model (data not shown). The level of radioactivity in the tumor increased for 120 min and then persisted at this level (SUV: 4.06 ± 0.51 at 120 min and 3.94 ± 1.01 at 240 min). The levels in the liver and kidney gradually decreased, while the lung, pancreas, spleen and small intestine showed a tendency to gradually increase and the uptake ratios of tumor to these organs were comparable between 120 and 240 min (SUV at 120 min: liver, 0.21 ± 0.02 ; kidney, 0.56 ± 0.05 ; lung, 0.89 ± 0.15 ; pancreas, 0.38 ± 0.03 ; spleen, 1.35 ± 0.06 ; and small intestine, 0.99 ± 0.12). Thus, it is expected that the static scan 110–120 min may provide good imaging contrast against surrounding normal tissues but the later scan may not improve the contrast.

Figure 1 shows the *ex vivo* autoradiograms of the liver of the metastasis model. There were many small nodules in the inferior lobes of the liver but few in the superior lobes. Even advanced high-resolution PET scanners may not be suitable for discriminating multiple small nodules.

Figure 2 shows the [^{18}F]FDG images and the time-activity curves in the dynamic PET scan of the metastasis tumor-bearing rat at 35 days after tumor inoculation. Immediately after injection of [^{18}F]FDG, the liver was visualized: the initial uptake of [^{18}F]FDG in the normal liver (superior lobe in the fifth slice, not shown) was higher than that in tumor, and the level in the normal liver

rapidly decreased. On the other hand, several hot spots including a large cluster of tumor nodules (8th slice) appeared in later images: the level in the tumor rapidly increased and reached a plateau at 90–120 min. However, PET could not discriminate numerous tumor nodules. The [¹⁸F]FDG uptake measured by PET was directly compared with that determined by the tissue dissection (Table 3). The SUV values in the normal liver region were comparable between PET and tissue dissection methods, while the tumor uptake evaluated by PET was much lower than that evaluated by tissue dissection. The finding demonstrated that the [¹⁸F]FDG uptake in the normal liver region was quantitatively evaluated by PET without the partial volume effect or the effects of the radioactivity in the thoracic organs. Although tumor was visualized as hot spots in all five rats investigated in the period investigated (5 weeks after tumor inoculation), we concluded that the PET signal in the tumor ROI was greatly influenced because of the partial volume effect and of the signal in the surrounding tissues.

Second, we examined the early detection of liver metastasis by static PET scans (110–120 min postinjection of [¹⁸F]FDG). As shown in Figure 3, at 18 days after tumor inoculation (group 4), [¹⁸F]FDG uptake in the liver region was relatively high compared with the control, but tumors were not clearly visualized as hot spots as observed in the rats in the group 5 (27 days after tumor inoculation). The finding represents that the PET scanner used could not visualize small multiple tumor nodules but detected their signals. Thus, the TVI concept was applied to these three groups for evaluation of [¹⁸F]FDG uptake instead of the SUV. Table 4 summarizes the TVIs values and the numbers of tumor nodules. Both indices were increased with time, but showed a large deviation as noted in Table 1. When the individual TVI values were plotted against the nodule numbers, there was a significant relationship between the two indices (Spearman, $r = 0.763$, $p < 0.002$) (Fig. 4). The finding suggests that the TVI reflects tumor volume or tumor viability, because these small tumor nodules had negligible necrotic regions. Only the nodules on the surface of the liver were counted, but not those inside, and the size of the nodules varied so greatly that the number of nodules did not accurately reflect tumor volume. Therefore, it is preferable that the TVI is compared with other tumor growth indices such as proliferating cell nuclear antigen.

A major problem for this method is that the ROI covering whole liver area in each splice were roughly located based on the PET images of dynamic scan and the photographs of anatomical slices of a few rats, but not based on the individual morphological images such as CT or MRI images. Due to the spatial resolution of the animal PET scanner used and the radioactivity in the surrounding organs such as the small intestine, pancreas and spleen, where [¹⁸F]FDG uptake was higher than that in the normal liver, the TVI values in the control group were not zero.

For location of the ROIs, a PET-MRI registration technique would be useful to overcome the problem.^{11,14} PET-CT scanners used clinically would be an other choice, if the high resolution is available. For the discrimination of the tumor activity from the surrounding tissues and for detection of numerous small nodules under 1 mm in diameter in the inferior lobes of the livers, however, even advanced high-resolution PET scanners may not be suitable, since it has been reported that they are capable of detecting only 35% of nodules under 2 mm in diameter.¹² On the other hand, the use of [¹⁸F]FDG uptake data in the normal liver region is reasonable. A region of normal liver was selected in the superior lobe of the liver, because there was no hot spot in the superior lobe of any of the groups investigated throughout the experimental period and because the superior lobe was found to be tumor-free at necropsy. Indeed both PET and tissue dissection methods gave similar SUV values for the [¹⁸F]FDG uptake in the normal liver (Table 3). Although a higher resolution PET scanner is preferable for more precise evaluation by TVI in any case, we successively evaluated tumor growth and the chemotherapeutic effects by TVI in the successive [¹⁸F]FDG-PET using the present metastasis model and the present PET scanner, the result is now under submission.

In conclusion, we have developed a liver metastatic tumor model and have proposed a new index, TVI, for evaluating tumor viability non-invasively and quantitatively by [¹⁸F]FDG-PET.

REFERENCES

1. Kubota K, From tumor biology to clinical PET: a review of positron emission tomography (PET) in oncology. *Ann Nucl Med* 2001; 15: 471–486.
2. Livraghi T. Guidelines for treatment of liver cancer. *Eur J Ultrasound* 2001; 13: 167–176.
3. Kokudo N, Imamura H, Sugawara Y, Sakamoto Y, Yamamoto J, Seki M, et al. Surgery for multiple hepatic colorectal metastases. *J Hepatobiliary Pancreat Surg* 2004; 11: 84–91.
4. Edward L. The detection of occult liver metastases of colorectal carcinoma. *J Hepatobiliary Pancreat Surg* 1999; 1: 7–15.
5. Kemeny N, Fata F. Arterial, portal, or systemic chemotherapy for patients with hepatic metastasis of colorectal carcinoma. *J Hepatobiliary Pancreat Surg* 1999; 1: 39–49.
6. Kubota K, Ishiwata K, Kubota R, Yamada S, Tada M, Sato T, et al. Tracer feasibility for monitoring tumor radiotherapy: a quadruple tracer study with fluorine-18-fluorodeoxyglucose or fluorine-18-fluorodeoxyuridine, L-[methyl-¹⁴C]methionine, [6-³H]thymidine, and gallium-67. *J Nucl Med* 1991; 32: 2118–2123.
7. Oyama N, Kim J, Jones LA, Mercer NM, Engelbach JA, Sharp TL, et al. MicroPET assessment of androgenic control of glucose and acetate uptake in the rat prostate and a prostate cancer tumor model. *Nucl Med Biol* 2002; 29: 783–790.

8. Yang H, Berger F, Tran C, Gambhir SS, Sawyers CL. MicroPET imaging of prostate cancer in LNCAP-SR39TK-GFP mouse xenografts. *Prostate* 2003; 55: 39–47.
9. Zanzonico P, O'Donoghue J, Chapman JD, Schneider R, Cai S, Larson S, et al. Iodine-124-labeled iodo-azomycin-galactoside imaging of tumor hypoxia in mice with serial microPET scanning. *Eur J Nucl Med Mol Imaging* 2004; 31: 117–128.
10. Chang CH, Fan KH, Chen TJ, Hsu WC, Jan ML, Tsai TH, et al. Dynamic evaluation of ¹⁸F-FDG uptake by microPET and whole-body autoradiography in a fibrosarcoma-bearing mouse model. *J Formos Med Assoc* 2004; 103: 876–881.
11. Rowland DJ, Garbow JR, Laforest R, Snyder AZ. Registration of [¹⁸F]FDG microPET and small-animal MRI. *Nucl Med Biol* 2005; 32: 567–572.
12. Kondo S, Hosono MN, Wada Y, Ishii K, Matsumura A, Takada Y, et al. Use of FDG-microPET for detection of small nodules in a rabbit model of pulmonary metastatic cancer. *Ann Nucl Med* 2004; 18: 51–57.
13. Ishiwata K, Kawamura K, Wang WF, Furumoto S, Kubota K, Pascali C, et al. Evaluation of *O*-[¹¹C]methyl-L-tyrosine and *O*-[¹⁸F]fluoromethyl-L-tyrosine as tumor imaging tracers by PET. *Nucl Med Biol* 2004; 31: 191–198.
14. Hayakawa N, Uemura K, Ishiwata K, Shimada Y, Ogi N, Nagaoka T, et al. A PET-MRI registration technique for PET studies of the rat brain. *Nucl Med Biol* 2000; 27:121–125.
15. Watanabe M, Uchida H, Okada H, Shimizu K, Satoh N, Yoshikawa E, et al. A high resolution PET for animal studies. *IEEE Trans Med Imag* 1992; 11: 577–580.
16. Inoue Y, Kashima Y, Aizawa K, Hatakeyama K. A new rat colon cancer cell line metastasizes spontaneously: biologic characteristics and chemotherapeutic response. *Jpn J Cancer Res* 1991; 82: 90–97.
17. Wang WF, Kiyosawa M, Ishiwata K, Mochizuki M. Glucose metabolism in the visual structures of rat monocularly deprived by eyelid suture after postnatal eye opening. *Jpn J Ophthalmol* 2005; 49: 6–11.